



Discrete sources method model for evanescent waves scattering analysis

Yuri Eremin^{a,*}, Thomas Wriedt^b

^a*Faculty of Applied Mathematics and Computer Science, Moscow State University, Lenin's Hills, 119992 Moscow, Russia*

^b*Institut für Werkstofftechnik, Badgasteiner Str. 3, 28359 Bremen, Germany*

Abstract

Discrete Sources Method has been extended to analyze P/S polarized evanescent waves scattering by a penetrable obstacle located on layered interface. Comparison strict model with the approximate one has been performed. Simulated results associated with synthesis of a metallic film enhances scattering of the evanescent wave has been presented.

© 2004 Elsevier Ltd. All rights reserved.

Keywords: Discrete sources method; Evanescent waves; Field enhancement

1. Introduction

The phenomenon of evanescent wave scattering has many potential applications. These include the total internal reflection microscopy [1], evanescent wave scattering measurements [2], characterization of thin films [3], and image of nano-structure reconstruction [4]. In particular employing an evanescent wave scattering in combination with surface plasmon resonance in the vicinity of metal-coated glass surface leads to image magnification [5]. In the past light scattering by penetrable particles has mainly been analyzed by approximate models. One of the most

*Corresponding author. Applied Mathematics and Computer Science Faculty, Moscow State University, Vorobyov Hills, Moscow 119899, Russian Federation. Tel.: +7-95-939-1776; fax: +7-95-939-2596.

E-mail addresses: eremin@cs.msu.su (Y. Eremin), thw@iwt.uni-bremen.de (T. Wriedt).

prevalent models applies Mie theory extended to the evanescent waves scattering. Such approach as a rule does not fully take into account particle–surface scattering interaction [6].

More recently Videen has developed a model that enables to consider light scattering partially accounting the interaction between particle and prism. This approach was valuable contribution to the theory of light scattering analysis [7]. In recent papers [8–10] computer model for evanescent wave scattering analysis has been developed based on the Discrete Sources Method (DSM). The model takes into account complete particle–interface interaction and provides an opportunity to investigate evanescent wave scattering by any axial symmetric obstacle near layered interface. In the present paper DSM will be applied to analyze evanescent waves scattering by penetrable particle deposited near a multi-layered interface. We will consider the results obtained by approximate model and strict DSM based model. We will investigate the conversion of evanescent wave into scattered waves by a penetrable particle deposited in the water near metal-coated glass prism. Based on computer simulation analysis we will treat the problem of optimal design of a metallic film and optimal choice of incident angle, which provide maximum enhancement of the scattered intensity in a required solid angle.

2. Discrete sources method

In this section the DSM model for evanescent wave scattering analysis is presented. We start with the mathematical statement of the polarized light scattering problem. Consider an axial symmetric penetrable particle with interior domain D_i and smooth boundary S is deposited above the plane surface Σ_f of a metallic film (Fig. 1). The film of thickness d occupying domain D_f is located on planar surface Σ_1 of a glass prism. We denote the prism domain by D_1 and ambient domain exterior to the particle by D_0 . Let us introduce Cartesian coordinate system $Oxyz$ by

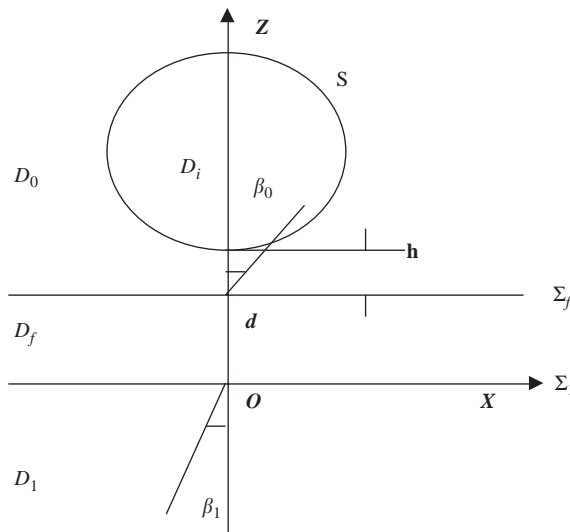


Fig. 1. Model geometry of a particle deposited on metal-coated glass surface.

choosing its origin O at the intersection point of the axis of symmetry of the particle and the plane Σ_1 . The Z -axis coincides with the axis of symmetry and is directed into domain D_0 . So that the planes $z = 0$ and d coincide with the Σ_1 and Σ_f planes, respectively.

We assume that exciting field $\{\mathbf{E}_1^i, \mathbf{H}_1^i\}$ is a linear polarized plane wave propagating from the glass prism at angle β_1 with respect to the Z -axis. According to the Snell's law wave $\{\mathbf{E}_0^i, \mathbf{H}_0^i\}$ refracted in D_0 propagates at angle β_0 to the Z -axis. Then the mathematical statement of the scattering problem can be formulated in the following form:

$$\begin{aligned} \nabla \times \mathbf{H}_\zeta &= jk\varepsilon_\zeta \mathbf{E}_\zeta, & \nabla \times \mathbf{E}_\zeta &= -jk\mu_\zeta \mathbf{H}_\zeta & \text{in } D_\zeta, & \zeta = 0, f, 1, i, \\ \mathbf{n} \times (\mathbf{E}_i - \mathbf{E}_0) &= 0, & \mathbf{n} \times (\mathbf{H}_i - \mathbf{H}_0) &= 0, & \text{at } S, \\ \mathbf{e}_z \times (E_0 - E_f) &= 0, & \mathbf{e}_z \times (H_0 - H_f) &= 0, & \text{at } \Sigma_f, \\ \mathbf{e}_z \times (E_f - E_1) &= 0, & \mathbf{e}_z \times (H_f - H_1) &= 0, & \text{at } \Sigma_1 \end{aligned} \quad (1)$$

and radiation (attenuation) conditions at infinity.

Here, \mathbf{n} is the outward unit normal vector to S , $k = \omega/c$ and $\{\mathbf{E}_\zeta, \mathbf{H}_\zeta\}$ stands for the total field in corresponding domain D_ζ . Note that the total field in D_0 is a superposition of the refracted exciting field and the scattered one, that is $\mathbf{E}_0 = \mathbf{E}_0^s + \mathbf{E}_0^i$, $\mathbf{H}_0 = \mathbf{H}_0^s + \mathbf{H}_0^i$. If $\text{Im } \varepsilon_\zeta, \mu_\zeta \leq 0$ (time dependence for the fields is chosen as $\exp\{j\omega t\}$) and the particle surface is smooth enough $S \subset C^{(1,2)}$ (Hölder space), then the above boundary-value problem is uniquely solvable.

We construct an approximate solution to the scattering problem (1) via the DSM by representing the electromagnetic fields as a finite linear combination of the fields of dipoles and multipoles which satisfy analytically transmission conditions enforced at the plane interfaces $\Sigma_{f,1}$ [10]. Then the approximate solution satisfies the Maxwell equations in the domains $D_\zeta, \zeta = 0, f, 1$, infinity conditions and the transmission conditions at the interfaces $\Sigma_{f,1}$. Eventually, the scattering problem is reduced to the problem of approximating the exciting field on particle surface S . The amplitudes of discrete sources are determined from the boundary conditions at the particle surface, which can be rewritten as

$$\mathbf{n} \times (\mathbf{E}_i - \mathbf{E}_0^s) = \mathbf{n} \times \mathbf{E}_0^i, \quad \mathbf{n} \times (\mathbf{H}_i - \mathbf{H}_0^s) = \mathbf{n} \times \mathbf{H}_0^i \quad \text{at } S. \quad (2)$$

To construct the fields of dipoles and multipoles satisfying analytically the transmission conditions at the plane interfaces $\Sigma_{f,1}$ we apply the Green's tensor for a stratified interface

$$\vec{\mathbf{G}}(\mathbf{r}, \mathbf{r}_0) = \begin{bmatrix} g^{e,h} & 0 & 0 \\ 0 & g^{e,h} & 0 \\ \frac{\partial f}{\partial x} & \frac{\partial f}{\partial y} & g^{h,e} \end{bmatrix}. \quad (3)$$

An approximate solution to the scattering problem is constructed fulfilling the transmission conditions on plane interfaces $\Sigma_{f,1}$, taking into account the rotational symmetry of the scattering problem geometry (particle plus layered interface) and polarization of the exciting field [10].

First, let us consider a P -polarized exciting field. In this case, the refracted plane wave in D_0 accepts the following form:

$$\begin{aligned} \mathbf{E}_0^i(\mathbf{r}) &= T^P(-\mathbf{e}_x \cos \beta_0 + \mathbf{e}_z \sin \beta_0) \exp\{-jk_0(x \sin \beta_0 + z \cos \beta_0)\}, \\ \mathbf{H}_0^i(\mathbf{r}) &= -T^P n_0 \mathbf{e}_y \exp\{-jk_0(x \sin \beta_0 + z \cos \beta_0)\}, \end{aligned} \tag{4}$$

where $(\mathbf{e}_x, \mathbf{e}_y, \mathbf{e}_z)$ are unit vectors of the Cartesian coordinate system, $n_0 = \sqrt{\varepsilon_0 \mu_0}$ and T^P is the transmission coefficient for P -polarization corresponding to multi-layered interface under consideration

$$T^{P,S} = \frac{T_{1f}^{P,S} T_{f0}^{P,S} \exp(jk_f \cos \beta_f d)}{1 + R_{1f}^{P,S} R_{f0}^{P,S} \exp(2jk_f \cos \beta_f d)}, \tag{5}$$

here $k_\zeta = k \sqrt{\varepsilon_\zeta \mu_\zeta}$, $\zeta = 0, f, 1$ and β_ζ is refractive angle inside a corresponding domain D_ζ , $\zeta = 0, f, 1$.

$$T_{\tau l}^P = \frac{2n_\tau \cos \beta_\tau}{n_\tau \cos \beta_l + n_l \cos \beta_\tau}, \quad R_{\tau l}^P = \frac{n_\tau \cos \beta_l - n_l \cos \beta_\tau}{n_\tau \cos \beta_l + n_l \cos \beta_\tau}$$

are the transmission and reflection Fresnel coefficients associated with interface between D_τ and D_l domains for the P -polarization [11]. If $\beta_l > \arcsin(n_0/n_l)$ the exciting wave is totally reflected from plane Σ_f and only an evanescent wave travelling along surface Σ_f and damped in the \mathbf{e}_z direction is present in D_0 . It follows from the Snell's law that in this case: hence, $\cos \beta_0$ becomes purely imaginary. We choose the value $\cos \beta_0 = -j\sqrt{\sin^2 \beta_0 - 1}$, since otherwise the amplitude of the refracted wave would tend to infinity with the increasing distance.

As mentioned above, the approximate solution to the scattering problem is constructed by taking into account not only the rotational symmetry of the scattering problem geometry, but also the polarization of the external excitation [12]. In this context, for P -polarized exciting plane wave (4) we use the following electric and magnetic vector potentials corresponding to the multipoles:

$$\begin{aligned} \mathbf{A}_{mm}^{e,0}(\mathbf{r}) &= \{g_m^e(\eta, z_n) \cos(m+1)\varphi; -g_m^e(\eta, z_n) \sin(m+1)\varphi; -f_{m+1}(\eta, z_n) \cos(m+1)\varphi\}, \\ \mathbf{A}_{mm}^{h,0}(\mathbf{r}) &= \{g_m^h(\eta, z_n) \sin(m+1)\varphi; g_m^h(\eta, z_n) \cos(m+1)\varphi; -f_{m+1}(\eta, z_n) \sin(m+1)\varphi\}, \\ \mathbf{A}_{0n}^{e,h,0}(\mathbf{r}) &= \{0; 0; g_0^{h,e}(\eta, z_n)\}, \end{aligned} \tag{6}$$

where $g_m^{e,h}, f_m$ are the Fourier harmonics relating to the Green tensor components, which accept the following form:

$$\begin{aligned} g_m^{e,h}(\eta, z_n) &= \int_0^\infty J_m(\lambda \rho) v_{11}^{e,h}(z, z_n, \lambda) \lambda^{1+m} d\lambda, \\ f_m(\eta, z_n) &= \int_0^\infty J_m(\lambda \rho) v_{31}(z, z_n, \lambda) \lambda^{1+m} d\lambda. \end{aligned} \tag{7}$$

Here J_m is the cylindrical Bessel function, (ρ, φ, z) are the cylindrical coordinates, point $\eta = (\rho, z)$ belongs to the semi-plane $\varphi = 0$, $R_{\eta z_n}^2 = \rho^2 + (z - z_n)^2$. While $\{z_n\}_{n=1}^\infty$ is a dense set of discrete source points distributed over a segment $\Gamma_z^0 \in D_i$ at the axis of symmetry, and $v_{11}^{e,h}(z, z_n, \lambda)$,

$v_{31}(z, z_n, \lambda)$ are the corresponding spectral functions. The spectral functions provide the continuity of the field tangential components at the interfaces $\Sigma_{f,1}$ can be represented as

$$v_{11}^{e,h} = \begin{cases} \frac{\exp\{-\eta_0|z - z_n|\}}{\eta_0} + A_{11}^{e,h}(\lambda, z_n) \exp\{-\eta_0|z - d|\}, & z \geq d, z_n > 0 \\ B_{11}^{e,h}(\lambda, z_n) \exp\{-\eta_f|z - d|\} + C_{11}^{e,h}(\lambda, z_n) \exp\{-\eta_f z\}, & d \geq z \geq 0; \\ D_{11}^{e,h}(\lambda, z_n) \exp\{\eta_1 z\}, & z \leq 0, \end{cases}$$

$$v_{31}^{e,h} = \begin{cases} A_{31}^{e,h}(\lambda, z_n) \exp\{-\eta_0|z - d|\}, & z \geq d, z_n > 0 \\ B_{31}^{e,h}(\lambda, z_n) \exp\{-\eta_f|z - d|\} + C_{31}^{e,h}(\lambda, z_n) \exp\{-\eta_f z\}, & d \geq z \geq 0; \\ D_{31}^{e,h}(\lambda, z_n) \exp\{\eta_1 z\}, & z \leq 0, \end{cases}$$

where $\eta_\zeta^2 = \lambda^2 - k_\zeta^2$, $\zeta = 0, f, 1$. Spectral coefficients A, B, C and D can be determined from the one dimensional transmission conditions at $z = 0, d$ which accepts the form [8]

$$[v_{11}^e] = \left[\frac{1}{\mu} \frac{\partial v_{11}^e}{\partial z} \right] = 0, \quad [v_{11}^h] = \left[\frac{1}{\varepsilon} \frac{\partial v_{11}^h}{\partial z} \right] = 0,$$

$$\left[\frac{1}{\mu} v_{31}^e \right] = 0, \quad \left[\frac{1}{\varepsilon \mu} \frac{\partial v_{31}^e}{\partial z} \right] = \left[\frac{1}{\varepsilon \mu} \right] v_{11}^e, \quad \left[\frac{1}{\varepsilon} v_{31}^h \right] = 0, \quad \left[\frac{1}{\varepsilon \mu} \frac{\partial v_{31}^h}{\partial z} \right] = \left[\frac{1}{\varepsilon \mu} \right] v_{11}^h.$$

In particular, the equality $v_{31}^e = v_{31}^h$ holds at $z \geq d$.

For the total field inside particle D_i we determine the following vector potentials [9]:

$$\mathbf{A}_{mm}^{e,i}(\mathbf{r}) = \{J_m^i(\eta, z_n) \cos(m+1)\varphi; -J_m^i(\eta, z_n) \sin(m+1)\varphi; 0\},$$

$$\mathbf{A}_{mm}^{h,i}(\mathbf{r}) = \{J_m^i(\eta, z_n) \sin(m+1)\varphi; J_m^i(\eta, z_n) \cos(m+1)\varphi; 0\},$$

$$\mathbf{A}_{0n}^{e,h,i}(\mathbf{r}) = \{0; 0; J_0^i(\eta, z_n)\}, \tag{8}$$

where $J_m^i(\eta, z_n) = j_m(k_i R_{\eta z_n})(\rho/R_{\eta z_n})^m$, and j_m are the spherical Bessel functions. Introduce the following notations:

$$\mathbf{R}_1^{\leftrightarrow \zeta} = \begin{pmatrix} j/k\varepsilon_\zeta \mu_\zeta & \nabla \times \nabla \times \\ -1/\mu_\zeta & \nabla \times \end{pmatrix}, \quad \mathbf{R}_2^{\leftrightarrow \zeta} = \begin{pmatrix} 1/\varepsilon_\zeta & \nabla \times \\ j/k\varepsilon_\zeta \mu_\zeta & \nabla \times \nabla \times \end{pmatrix}. \tag{9}$$

Now, we can represent the approximate solution to the scattering problem for the P -polarized excitation as [12]

$$\begin{pmatrix} \mathbf{E}_N^\zeta \\ \mathbf{H}_N^\zeta \end{pmatrix} = \sum_{m=0}^M \sum_{n=1}^{N_m^\zeta} \left\{ p_{mn}^\zeta \mathbf{R}_1^{\leftrightarrow \zeta} \mathbf{A}_{mn}^{e,\zeta} + q_{mn}^\zeta \mathbf{R}_2^{\leftrightarrow \zeta} \mathbf{A}_{mn}^{h,\zeta} \right\} + \sum_{n=1}^{N_n^\zeta} r_n^\zeta \mathbf{R}_1^{\leftrightarrow \zeta} \mathbf{A}_n^{e,\zeta}, \quad \zeta = 0, i. \tag{10}$$

The last term in (10) is associated with vertical electric dipoles. Here, N is a complex index incorporating M and N_m^ζ . Let us emphasize that in frame of the DSM, scattered field $\{\mathbf{E}_N^\zeta, \mathbf{H}_N^\zeta\}$ in domains $D_{0,f,1}$ can be represented in terms of the unitary set of amplitudes $\{p_{mn}^0, q_{mn}^0, r_n^0\}$ after the transmission conditions at the interfaces Σ_f and Σ_1 are satisfied using Green's tensor components (7) [12].

Consider now *S*-polarization of the exciting plane wave

$$\mathbf{E}_0^i(\mathbf{r}) = T^S \mathbf{e}_y \exp\{-jk_0(x \sin \beta_0 + z \cos \beta_0)\}$$

$$\mathbf{H}_0^i(\mathbf{r}) = T^S n_0(-\mathbf{e}_x \cos \beta_0 + \mathbf{e}_z \sin \beta_0) \exp\{-jk_0(x \sin \beta_0 + z \cos \beta_0)\}, \tag{11}$$

where T^S is given by (5) and associated Fresnel coefficients accept the following form [11]:

$$T_{\tau l}^S = \frac{2n_\tau \cos \beta_\tau}{n_\tau \cos \beta_\tau + n_l \cos \beta_l}, \quad R_{\tau l}^S = \frac{n_l \cos \beta_l - n_\tau \cos \beta_\tau}{n_l \cos \beta_l + n_\tau \cos \beta_\tau}$$

To take into account polarization of the external excitation for *S*-polarized plane wave (11) we should use the following electric and magnetic potentials:

$$\mathbf{A}_{mn}^{e,0}(\mathbf{r}) = \{g_m^e(\eta, z_n) \sin(m + 1)\varphi; g_m^e(\eta, z_n) \cos(m + 1)\varphi; -f_{m+1}(\eta, z_n) \sin(m + 1)\varphi\},$$

$$\mathbf{A}_{mn}^{h,0}(\mathbf{r}) = \{g_m^h(\eta, z_n) \cos(m + 1)\varphi; -g_m^h(\eta, z_n) \sin(m + 1)\varphi; -f_{m+1}(\eta, z_n) \cos(m + 1)\varphi\},$$

$$\mathbf{A}_{0n}^{e,h,0}(\mathbf{r}) = \{0; 0; g_0^{h,e}(\eta, z_n)\}; \tag{12}$$

So, for *S* polarization the approximate solution accept the following form:

$$\begin{pmatrix} \mathbf{E}_N^\zeta \\ \mathbf{H}_N^\zeta \end{pmatrix} = \sum_{m=0}^M \sum_{n=1}^{N_m^\zeta} \{p_{mn}^\zeta \mathbf{R}_1 \mathbf{A}_{mn}^{e,\zeta} + q_{mn}^\zeta \mathbf{R}_2 \mathbf{A}_{mn}^{h,\zeta}\} + \sum_{n=1}^{N_m^\zeta} r_n^\zeta \mathbf{R}_2 \mathbf{A}_n^{h,\zeta}; \quad \zeta = 0, i. \tag{13}$$

The last term in (13) is associated with vertical magnetic dipoles [12]. The difference between (10) and (13) is caused by the fact that for *S*-polarization vector \mathbf{H}_0^i belongs to the incident plane.

The completeness of the system of lowest-order distributed multipoles used in (10) and (13) guarantees the convergence of the approximate solution to the exact one in any closed subset of D_0 [12].

As mentioned above representations (10) and (13) satisfies all the conditions of scattering problem (1) except the transmission conditions at the particle surface (2). These conditions are employed to determine amplitudes of discrete sources $\{p_{mn}^{0,i}, q_{mn}^{0,i}, r_n^{0,i}\}$. Since the scattering problem geometry is axially symmetric with respect to the *Z*-axis and discrete sources are distributed over the axis of symmetry, fulfilling the transmission conditions (2) at surface *S* can be reduced to the sequential solution of the transmission problems for the Fourier harmonics of the fields. So, instead of matching the fields on the scattering surface (see (2)), we can match their Fourier harmonics thus reducing approximation problem on the surface to a set of the problems enforced at the particle surface generatrix \mathfrak{S} . By solving these problems one can determine the discrete sources amplitudes $\{p_{mn}^{0,i}, q_{mn}^{0,i}, r_n^{0,i}\}$.

Various numerical schemes for determination of the amplitudes are at our disposal. It has been found that stable results can be obtained by using the generalized point-matching technique and pseudo-solution of an over-determined system of linear equations [13]. The DSM is a direct method and hence it allows one to solve the scattering problem for the entire set of incident angles β_1 and both polarizations (*P* and *S*) at once. Besides, the numerical scheme provides an opportunity to control the convergence of the approximate solution by posterior error estimation [12].

After the amplitudes of discrete sources are determined, one can calculate far-field pattern $E_\infty(\theta, \phi)$ of the scattered field, which is determined at the upper part of the unit semi-sphere $\Omega = \{0^\circ \leq \theta < 90^\circ, 0^\circ \leq \phi \leq 360^\circ\}$ and is given by

$$E_\infty^S(\mathbf{r})/|E^0(z=0)| = \frac{\exp\{-jk_0R\}}{R} E_\infty(\theta, \phi) + O(R^{-2}), \quad R = |\mathbf{r}| \rightarrow \infty, z > 0.$$

We asymptotically estimate the Weyl–Sommerfeld integrals involved in (7) [12], which yields to the following representation for the θ, φ -components of the far-field pattern corresponding to representation (10)

$$E_{\infty,\theta}^P(\theta, \varphi) = jk_0 \sum_{m=0}^M \cos(m+1)\varphi(j \sin \theta)^m \sum_{n=1}^{N_m^0} \{p_{nm}^0 \cos \theta [f'_n + (v_n^e - v_n \sin^2 \theta)f_n] + q_{nm}^0(f'_n + v_n^h f_n)\} - jk_0 \sin \theta \sum_{n=1}^{N_m^0} r_n^0(f'_n + v_n^h f_n),$$

$$E_{\infty,\varphi}^P(\theta, \varphi) = -jk_0 \sum_{m=0}^M \sin(m+1)\varphi(j \sin \theta)^m \sum_{n=1}^{N_m^0} \{p_{nm}^0(f'_n + v_n^e f_n) + q_{nm}^0 \cos \theta \times [f'_n + (v_n^h - v_n \sin^2 \theta)f_n]\} \tag{14}$$

For S -polarized excitation following to representation (13) one can get:

$$E_{\infty,\theta}^S(\theta, \varphi) = jk_0 \sum_{m=0}^M \sin(m+1)\varphi(j \sin \theta)^m \sum_{n=1}^{N_m^0} \{p_{nm}^0 \cos \theta [f'_n + (v_n^e - v_n \sin^2 \theta)f_n] - q_{nm}^0(f'_n + v_n^h f_n)\}$$

$$E_{\infty,\varphi}^S(\theta, \varphi) = jk_0 \sum_{m=0}^M \cos(m+1)\varphi(j \sin \theta)^m \sum_{n=1}^{N_m^0} \{p_{nm}^0 \cos \theta [f'_n + (v_n^e - v_n \sin^2 \theta)f_n] - q_{nm}^0(f'_n + v_n^h f_n)\} + jk_0 \sin \theta \sum_{n=1}^{N_m^0} r_n^0(f'_n + v_n^e f_n), \tag{15}$$

where corresponding spectral functions are

$$v_n^{e,h}(\theta, z_n) = jk_0 \cos \theta \exp\{jk_0 d \cos \theta\} A_{11}^{e,h}(k_0 \sin \theta, z_n)$$

$$v_n(\theta, z_n) = jk_0 \cos \theta \exp\{jk_0 d \cos \theta\} A_{31}(k_0 \sin \theta, z_n)$$

and

$$f_n = \exp\{-jk_0 z_n \cos \theta\}, \quad f'_n = \exp\{jk_0 z_n \cos \theta\}.$$

Hence, after the unknown amplitudes of discrete sources are determined, far-field pattern for P/S polarization (14, 15) are represented as finite linear combinations of elementary functions.

This circumstance ensures economical computer analysis of the scattering characteristics in the wave zone.

3. Results and discussion

In this section we consider computer simulation results associated with conversion evanescent waves into scattered ones by a particle deposited on a metal-filmed glass prism. We consider the Differential Scattering Cross-Section (DSC), which is given by

$$DSC^{P,S}(\beta_1, \theta, \varphi) = |E_{\infty,\theta}^{P,S}(\beta_1, \theta, \varphi)|^2 + |E_{\infty,\varphi}^{P,S}(\beta_1, \theta, \varphi)|^2 \tag{16}$$

Here $E_{\infty,\theta,\varphi}^{P,S}(\theta, \varphi)$ are the components of the far-field pattern (14–15) corresponding to the P/S -polarized excitation measured in μm^2 . We compute an integral response

$$L^{P,S}(\beta_1) = \int_{\bar{\Omega}} DSC^{P,S}(\beta_1, \theta, \varphi) d\omega, \tag{17}$$

which represents intensity scattered in a certain solid angle $\bar{\Omega}$. The integral response is used to evaluate scattered intensity captured by lens immersed in water [14].

We examine the exciting plane wave at the wavelength in free space $\lambda = 488 \text{ nm}$. Let the glass prism have the refractive index of $n_1 = 1.52$. Assume that a particle with refractive index $n_i = 1.59$ is located in water characterized by refractive index $n_0 = 1.33$. So, an evanescent wave appears at incident angles $\beta_1 > \beta_c$ where critical angle $\beta_c = \arcsin(n_0/n_1)$ and for our particular case $\beta_c \approx 61.05^\circ$. Consider a plane wave propagating from prism side in this case $90^\circ > \beta_1 \geq 0^\circ$ and $\beta_{f,0}$ can be determined using the Snell’s law. Recall that $\beta_1 = 0^\circ$ corresponds to a plane wave propagating normally to the prism surface.

We start with the comparison strict DSM model with approximate one similar to [7], which based on Fresnel approximation for Weil–Sommerfeld integrals (7). Consider glass prism covered by silver film of thickness $d = 45 \text{ nm}$ characterized by the complex refractive index $n_f = 0.13 - 2.82j$. Fig. 2 demonstrates $DSC^{P,S}$ versus scattering angle in the incident plane for

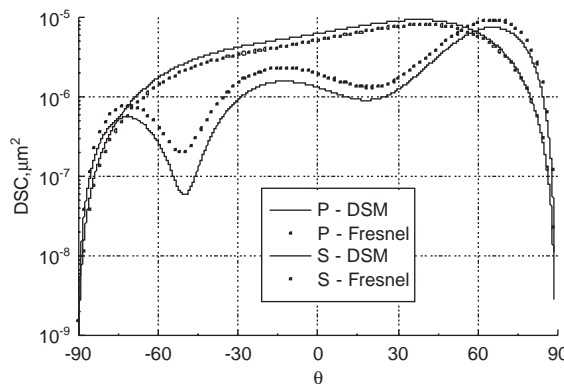


Fig. 2. $DSC^{P,S}$: (16) (in μm^2) versus scattering θ (in degrees) in the incident plane. Incident angle $\beta_1 = 62^\circ$.

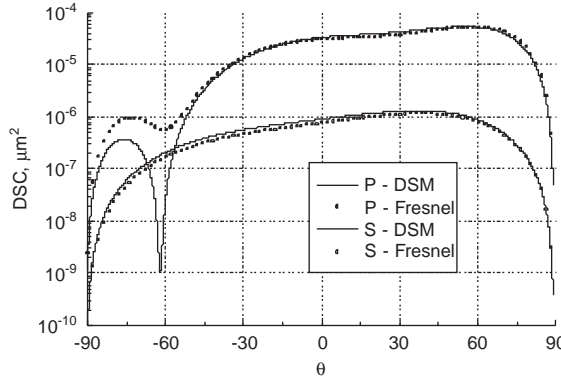


Fig. 3. The same as in Fig. 2 results, but for incidence $\beta_1 = 70^\circ$.

spherical particle $D = 150$ nm and incident angle $\beta_1 = 62^\circ$. Fig. 3 shows the same results but for incidence $\beta_1 = 70^\circ$. One can see visible deviation of the results especially for P -polarized light, which can reach several orders of magnitude at some scattering angles.

One of the specific features of the schemes involved in express diagnosis, which is applied to detect of bacteria or viruses in solutions, is the presence of metallic film on the glass surface. For this purpose various metals such as aluminium, copper, silver and gold can be used [5]. The film thickness varies from 10 to 100 nm. To investigate this effect and optimize the incident field parameters and film thickness (β_1, d) we analyze the following quantity:

$$E^{P,S}(\beta_1, d) = \frac{|T^{P,S}|^2}{|T_{01}^{P,S}|^2}, \quad (18)$$

where $T^{P,S}$ is the transmission coefficient for the metal-filmed prism expressed by (5) and $T_{01}^{P,S}$ coefficient corresponds to the case $d = 0$. Quantity $E^{P,S}$ represents the coefficient of evanescent wave amplification due to the presence of a metal film. In this case, it has been found that silver film is the most suitable (aluminium, copper, silver and gold have been treated). The results associated with the enhancement and reflectivity of the structure $r^P = |R^P|^2$ where

$$R^{P,S} = \frac{R_{1f}^{P,S} + R_{f0}^{P,S} \exp(2jk_f \cos \beta_f d)}{1 + R_{1f}^{P,S} R_{f0}^{P,S} \exp(2jk_f \cos \beta_f d)} \quad (19)$$

are depicted on Fig. 4. One can see that in the vicinity of a sharp minimum of the reflectivity enhancement reaches a maximum value. But at the same time the value of the enhancement is much smaller than one can expect from the reflectivity curve. It is a consequence that some part of energy be absorbed inside the film. The same results for gold film are demonstrated in Fig. 5. The results are agreed with [15].

Fig. 6 shows E^S versus incident angle β_1 at various values of the film thickness. Salient point of the curves corresponds to the critical angle β_c . One can conclude that S polarized excitation does not reveal any enhancement of the evanescent wave behind the critical angle.

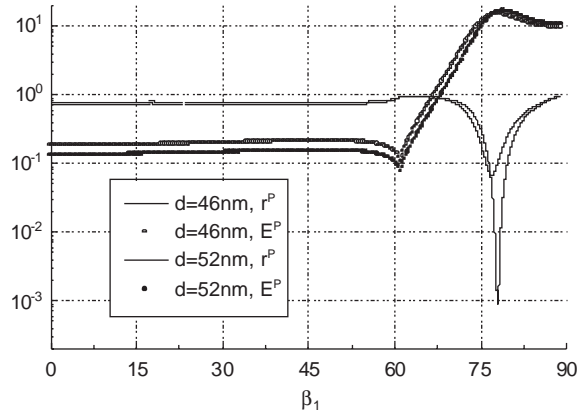


Fig. 4. Enhancement E^P and reflectivity r^P versus incident angle β_1 . Two silver film thicknesses $d = 46, 52$ nm are considered.

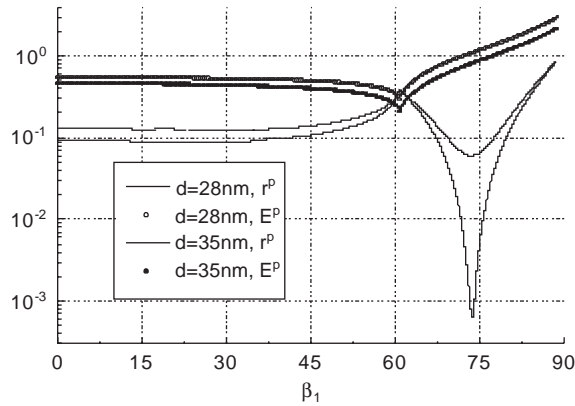


Fig. 5. The same as in Fig. 4 results, but for incidence gold film. Two film thicknesses $d = 28, 35$ nm are considered.

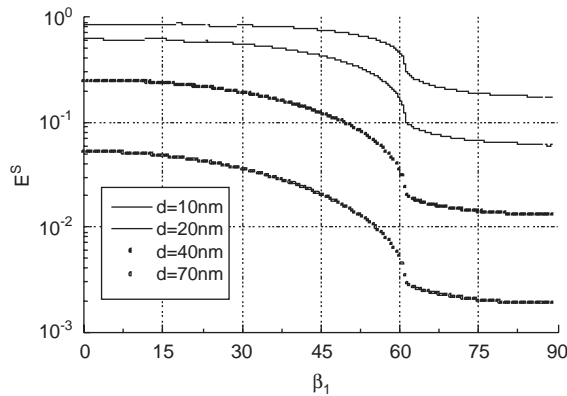


Fig. 6. E^S versus incident angle. Four silver film thicknesses $d = 10, 20, 40, 70$ nm are considered.

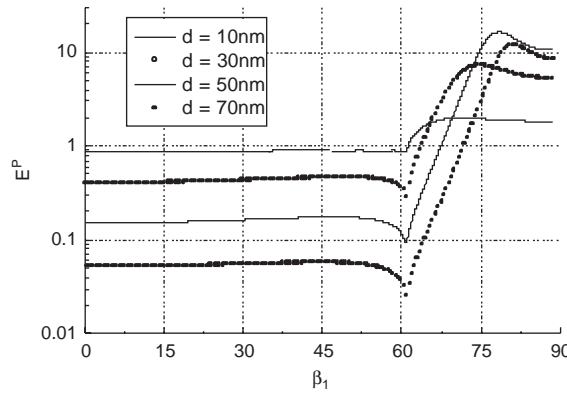


Fig. 7. E^P versus incident angle. Four silver film thicknesses $d = 10, 30, 50, 70$ nm are considered.

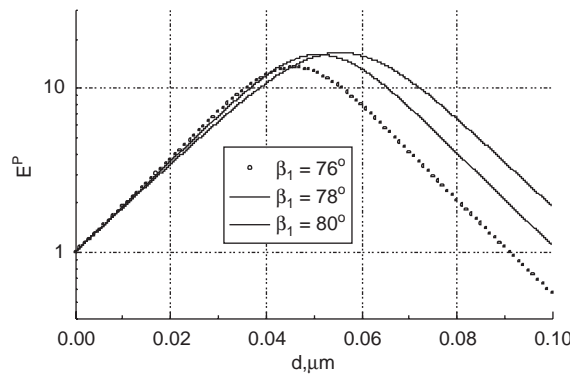


Fig. 8. E^P versus Ag film thickness. Three incident angles $\beta_1 = 76^\circ, 78^\circ$ and 80° are considered.

Fig. 7 demonstrates the results for P polarized enhancement E^P . It is clear that the maximum value of the intensity enhancement is attained in the vicinity of the point $\beta_1 = 78^\circ$ and exceeds a value of 10.

The dependence of E^P on film thickness d is depicted in the Fig. 8 at several incident angles. The investigation performed allows one to choose “optimal” values for (β_1, d) . Therefore, it seems reasonable to choose the film thickness $d = 50$ nm and incident angle $\beta_1 = 78^\circ$ as a basis for the following specification.

In Fig. 9, we plot the integral response of a spherical particle of the diameter $D = 50$ nm corresponding to the solid angle $\bar{\Omega} = \{37.5^\circ \geq \theta \geq 0^\circ; 360^\circ > \varphi \geq 0^\circ\}$. It is assumed that the lens is embedded in water far from the interface [5]. These results obtained using DSM model enable us to correct the optimal values for (β_1, d) found at the first stage of the investigation. In Fig. 9 one can see that the film thickness $d = 32$ nm and incident angle $\beta_1 = 75^\circ$ provide a higher integral response. This circumstance means that interaction between the field scattered by a particle and a multi-layered interface plays a key role and must be taken into account.

Fig. 10 demonstrates the integral response versus of the particle diameter. Results for a spherical particle and equivolume prolate and oblate spheroids with axes ratio 1.5 are depicted. It is clear that the optimal values work rather well up to the particle diameter $D = 150$ nm.

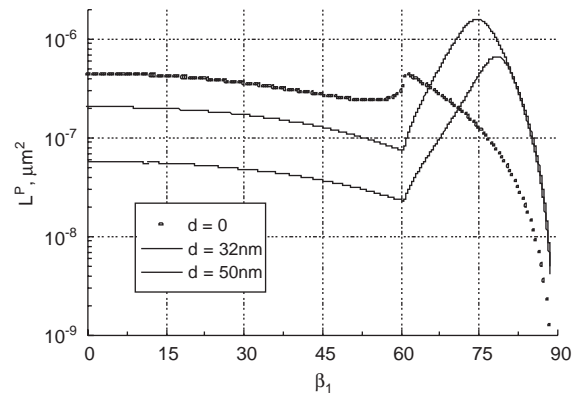


Fig. 9. Integral response L^P : (17) (in μm^2) versus incident angle β_1 for spherical particle $D = 50$ nm. Three values of film thickness $d = 0$, 32 and 50 nm are considered.

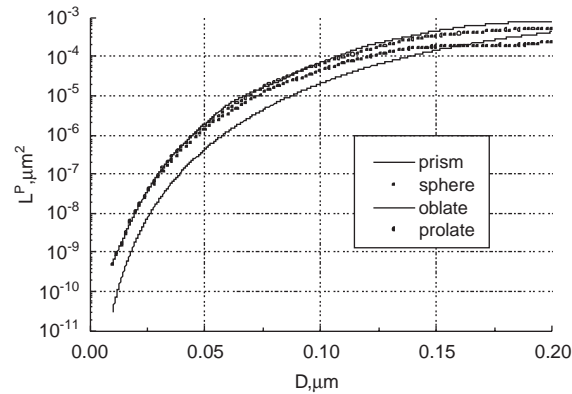


Fig. 10. Integral response versus particle equivolume diameter. Responses for $d = 0$, $\beta_1 = 62^\circ$ and $d = 32$ nm, $\beta_1 = 75^\circ$ (sphere, oblate and prolate spheroids) are considered.

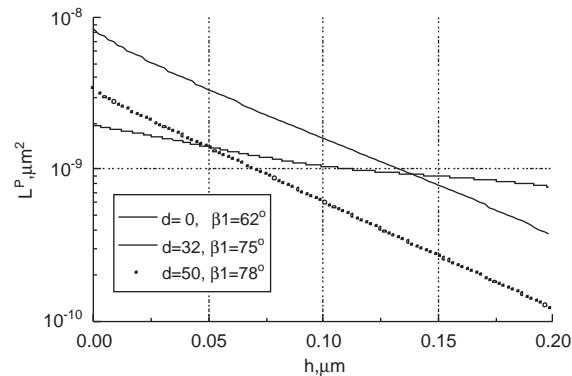


Fig. 11. Integral response versus distance between spherical particle $D = 20$ nm and the interface. Responses for $d = 0$, $\beta_1 = 62^\circ$; $d = 32$ nm, $\beta_1 = 75^\circ$ and $d = 50$ nm, $\beta_1 = 78^\circ$ are considered.

In Fig. 11 the integral response corresponding to the different values of (β_1, d) versus the distance between spherical particle and the interface is depicted. One can see that the optimal values provide higher response up to distance of 130 nm.

4. Conclusion

Based on the Discrete Sources Method, computer model for analysis of the evanescent waves scattering by a non-spherical particle located near a metal-coated glass prism has been developed. The optimal value of (β_1, d) providing the maximum lens response has been accomplished. It has been shown that the interaction between the field scattered by a particle and a multi-layered interface plays a key role and must be taken into account in any theoretical model.

Acknowledgements

We gratefully acknowledge funding of this research by Deutsche Forschungsgemeinschaft (DFG) and the Russian Foundation for Basic Research (RFBR).

References

- [1] Girard Ch, Dereux A. Near-field optics theories. *Rep Prog Phys* 1996;59:657–99.
- [2] Schumacher GA, Vandeven TG. Evanescent wave scattering studies on latex-glass interactions. *Langmuir* 1991;7:2028–33.
- [3] Kitson SC, Sambles JR. Critical edge study highly absorbing anisotropic films. *Thin Solid Films* 1993:128–32.
- [4] Ohiem M. Review: Imaging transmitter release. II A practical guide to evanescent-wave imaging. *Lasers Med Sci* 2001;16:159–70.
- [5] Ganic D, Gan X, Gu M. Three-dimensional evanescent wave scattering by dielectric particles. *Optik* 2002;113(3):135–41.
- [6] Quinten M, Pack A, Wannemacher R. Scattering and excitation of evanescent waves by small particles. *Appl Phys B* 1999;68:87–93.
- [7] Videen G. Light scattering from a sphere on or near a surface. *J Opt Soc Am A* 1991;8:483–9.
- [8] Doicu A, Eremin Yu A, Wriedt T. Scattering of evanescent waves by a particle on or near a plane surface. *Comput Phys Commun* 2001;134:1–10.
- [9] Doicu A, Eremin Yu A, Wriedt T. Scattering of evanescent waves by a sensor tip near a plane surface. *Opt Commun* 2001;190:5–12.
- [10] Eremin Yu A, Wriedt T. Large dielectric non-spherical particle in an evanescent wave field near a plane surface. *Opt Commun* 2002;214:39–45.
- [11] Chew WC. *Waves and fields in inhomogeneous media*. New York; 1990.
- [12] Eremin Yu A, Orlov NV, Sveshnikov AG. Models of electromagnetic scattering problems based on discrete sources methods. In: Wriedt T, editor. *Generalizes multipole techniques for electromagnetic and light scattering*. Amsterdam: Elsevier Science; 1999. p. 39–79.
- [13] Voevodin VV, Kuznetsov Yu A. *Matrixes and computations*. Moscow: Science Press; 1984 (in Russian).
- [14] Enderlein J. A theoretical investigation of single-molecule fluorescence detection on thin metallic layers. *Biophys J* 2000;78:2151–8.
- [15] Reather H. *Surface plasmons*. Springer: Berlin; 1988 [chapter 2].